

RESEARCH ARTICLE

EMU Radio Observations of Barred Spiral Galaxy NGC 5938 (Araish)

H. Zakir,¹ M.D. Filipović,¹ L. Barnes,¹ R. Z. E. Alsaberi,^{2,1} T. An,^{3,4} K. Dage,⁵ S. W. Duchesne,⁶ A. M. Hopkins,⁷ A. Kapinska,⁸ B. Koribalski,^{9,1} S. Lazarević,^{1,9,10} D. Leahy,¹¹ Z. Liu,¹² R. P. Norris,^{9,1} A. Rau,¹² Z.J. Smeaton,¹ and T. Jarrett*^{13,1,14}

¹School of Science, Western Sydney University, Locked Bag 1797, Kingswood, 2751, NSW, Australia

²Faculty of Engineering, Gifu University, 1-1 Yanagido, Gifu 501-1193, Japan

³Shanghai Astronomical Observatory, CAS, 80 Nandan Road, Shanghai 200030, P.R. China

⁴State Key Laboratory of Radio Astronomy and Technology, A20 Datun Road, Chaoyang District, Beijing, P. R. China

⁵Curtin Institute of Radio Astronomy, Curtin University: Perth, Western Australia, AU

⁶Australia Telescope National Facility, CSIRO, Space and Astronomy, PO Box 1130, Bentley, WA 6151, Australia

⁷School of Mathematical and Physical Sciences, Macquarie University, 12 Wally's Walk, Macquarie Park, 2109, NSW, Australia

⁸National Radio Astronomy Observatory (NRAO), 1011 Lopezville Rd, Socorro NM 87801, USA

⁹Australia Telescope National Facility, CSIRO, Space and Astronomy, PO Box 76, Epping, NSW 1710, Australia

¹⁰Astronomical Observatory, Volgina 7, 11060 Belgrade, Serbia

¹¹Department of Physics and Astronomy, University of Calgary, Calgary, Alberta, T2N 1N4, Canada

¹²Max Planck Institute for extraterrestrial Physics, Giessenbachstr. 1, 85748 Garching, Germany

¹³Department of Astronomy, University of Cape Town, Private Bag X3, Rondebosch 7701, South Africa

¹⁴* Deceased on 3 July 2024

Author for correspondence: Hina Zakir, Email: 22110114@student.westernsydney.edu.au.

Abstract

We present multi-wavelength observations of the nearby spiral galaxy NGC 5938 (Araish) to investigate the origin of its radio emission, specifically the contribution from active galactic nucleus (AGN) activity and star formation. Using Evolutionary Map of the Universe (EMU) data, we detect extended radio emission extending outwards to the galactic axis, with a steep non-thermal spectral index ($\alpha = -1.2 \pm 0.2$) indicative of synchrotron radiation from an AGN jet. The jet has a physical extent of ≈ 8.2 kpc (angular length of $64''$). Multi-wavelength data from The Dark Energy Camera Plane Survey 2 (DECaPS2), Wide-field Infrared Survey Explorer (WISE), and extended Roentgen Survey with an Imaging Telescope Array (eROSITA) provide further support for this interpretation. The colour-colour diagram presenting WISE infrared observations suggests the presence of dust and young stars that trace the galaxy's disk structure. Our analysis reveals a radio jet, alongside star formation traced by infrared emission, demonstrating the complex interplay of AGN activity and star formation in this well-resolved galaxy. Intriguingly, the spatial relationship reveals the brighter X-ray emission to be largely adjacent to and enveloping the extended radio emission. This suggests that the radio jet, while extending at a significant angle to the galactic disk, is confined by the larger X-ray gas/halo, similar to other systems (i.e., ESO 295-IG022, Centaurus A) and may indicate jet collimation and channelling effects.^a

Keywords: NGC 5938 — ASKAP — EMU — SFMS — Star formation — AGN — NGC 5938 — ESO 295-IG022 — NGC 1068

^aAccepted for publication in PASA.

1. Introduction

Radio emission in galaxies can originate from multiple astrophysical processes, primarily driven by compact objects such as supernova remnants (SNRs), massive star-forming regions, or central supermassive black holes (SMBHs) producing active galactic nucleus (AGN). In particular, AGN-driven jets emit strongly at radio wavelengths via synchrotron radiation and can significantly influence galaxy evolution by regulating star formation through feedback processes (Best & Heckman, 2012; Fabian, 2012). However, disentangling AGN activity from star formation in galaxies, especially at average resolutions, remains challenging, as both can contribute substantially to the total radio output (Mauch & Sadler, 2007).

While powerful radio jets are commonly observed in elliptical galaxies or massive quasars, their presence in spiral galaxies is rare. These systems, often referred to as spiral Double Radio-source Associated with Galactic Nucleus (DRAGN; Mao et al., 2018; Singh et al., 2015; Norris et al., 2025), represent a unique class where classical disk morphology coexists with large-scale

radio jets (Gao et al., 2023). Spiral DRAGNs challenge traditional paradigms of AGN-hosting environments and raise important questions about jet triggering mechanisms, gas accretion histories, and the role of galaxy mergers in otherwise secularly evolving systems.

Notable examples include 0313-192 (Ledlow et al., 2001), a massive edge-on spiral galaxy with a radio jet of ≈ 300 kpc, and NGC 3079, a barred spiral hosting a compact radio outflow and kpc-scale X-ray bubble (Cecil et al., 2001). The Circinus Galaxy (Elmouttie et al., 1998), although not formally classified as a DRAGN, hosts Seyfert-like nuclear activity, a starburst ring, and collimated radio structures. These systems serve as critical laboratories for probing the interplay between star formation, AGN feedback, and interstellar medium (ISM) dynamics in non-elliptical hosts.

In this paper, we present new multi-wavelength observations of NGC 5938, an edge-on spiral galaxy exhibiting prominent radio emission suggestive of AGN-driven activity. Observations were obtained as part of the Evolutionary Map of

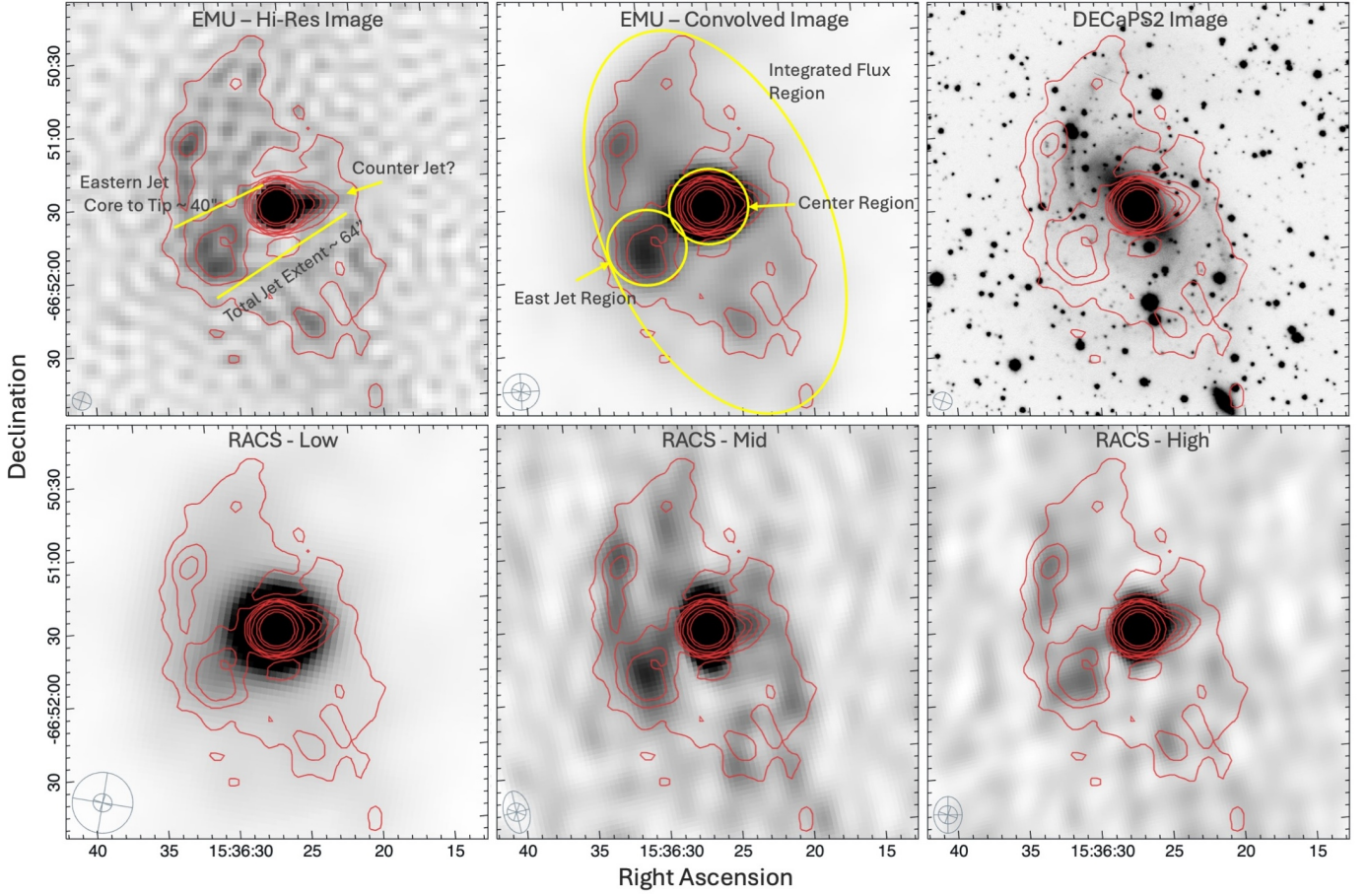


Figure 1. Radio and NIR observations of NGC 5938 (Araish). The top row (from left to right) shows the EMU Hi-Res image, the EMU Convolved Image, and the DECaPS2 optical z-band image. The bottom row shows the RACS Low, RACS Mid, and RACS High band images with the EMU Hi-Res contours overlaid at 3, 6, 9, 12, 15, 25, 50, and 75 σ on all panels, where $\sigma = 65 \mu\text{Jy beam}^{-1}$.

the Universe (EMU; Norris et al., 2021; Hopkins et al., 2025) survey conducted with the Australian Square Kilometre Array Pathfinder (ASKAP; Hotan et al., 2021). Despite its regular spiral appearance, it shows extended radio emission over a projected extent of $\sim 33''$ (≈ 4.2 kpc), consistent with structures commonly associated with AGN activity (Cielo et al., 2017). Among the possible mechanisms responsible for this emission are an extended radio jet or a compact radio lobe, similar to those observed in nearby systems such as NGC 3079 (Cecil et al., 2001), where a kpc-scale radio outflow emerges from the disk.

We also use complementary observations from the Wide-field Infrared Survey Explorer (WISE; Wright et al., 2010), The Dark Energy Camera Plane Survey 2 (DECaPS2; Sayd-jari et al., 2023), and the extended Roentgen Survey with an Imaging Telescope Array (eROSITA; Predehl et al., 2021) to examine the interplay between the radio jet and star formation, as traced by infrared and X-ray emission. The spatial morphology and multi-wavelength signatures of NGC 5938 place it among the rare class of spiral galaxies with AGN-driven outflows, as visible in NGC 1068 (Young et al., 2001; Cecil et al., 2002).

NGC 5938 is nicknamed *Araish*, a word meaning “adorn-

ment” in Urdu, reflecting the galaxy’s striking spiral morphology and active star-forming disk. This visual impression, particularly the representation of its orderly disk and the emerging radio jet, motivated the informal use of this name in the manuscript.

A detailed characterisation of the target galaxy is provided in Section 2. The observational data are described in Section 3, followed by an analysis of the jet and host morphology in Section 4.1. Our findings are described in the context of similar systems in Section 4 and we conclude with a summary of the implications for spiral galaxies exhibiting both AGN and star-formation signatures.

2. Target Description: NGC 5938 (Araish)

NGC 5938 is a nearby barred spiral galaxy located at $\text{RA} = 15^{\text{h}}36^{\text{m}}18^{\text{s}}$, $\text{Dec} = -66^{\circ}13'47''$ (J2000), and is catalogued in multiple surveys, including the HI Parkes All-Sky Survey (HIPASS), as HIPASS J1536–66 (Koribalski et al., 2004). It exhibits a well-defined disk morphology with B, R, and I band magnitudes of 11.9, 12.0, and 11.5, respectively (Doyle et al., 2005). Despite its regular spiral appearance, it shows extended radio emission consistent with a radio lobe or jet. Such features are rare among spiral galaxies and are commonly clas-

sified as spiral DRAGNs, a class that challenges the traditional view that large-scale radio jets occur only in elliptical hosts (Gao et al., 2023). These galaxies serve as valuable laboratories for studying the interplay of AGN feedback and disk galaxy evolution.

NGC 5938 has a redshift of $z = 0.012$, corresponding to a systemic $\text{H}\alpha$ velocity of $v_{\text{sys}} = 3512 \pm 9 \text{ km s}^{-1}$ (Koribalski et al., 2004). In the Local Group frame, the velocity becomes $v_{\text{LG}} = 3314 \text{ km s}^{-1}$. A simple application of the Hubble–Le maître law with $H_0 = 75 \text{ km s}^{-1} \text{ Mpc}^{-1}$ yields a Hubble-flow distance of $\sim 44.2 \text{ Mpc}$. However, redshift-based distances are uncertain at such low redshift values due to large peculiar motions (Terry et al., 2002).

To derive a more accurate distance, we apply redshift-independent methods. The *sosie* galaxy technique (Theureau et al., 2007) and the Tully–Fisher relation (Steer, 2020) both yield consistent values of $\sim 26.6 \pm 0.4 \text{ Mpc}$ and $\sim 26 \text{ Mpc}$, respectively. We adopt the *sosie* galaxy distance of 26.6 Mpc for all physical calculations in this work.

NGC 5938 contains a substantial neutral hydrogen reservoir with $\text{H}\alpha$ flux of $F_{\text{H}\alpha} = 26.4 \pm 3.7 \text{ Jy km s}^{-1}$ and a derived $\text{H}\alpha$ mass of $\log(M_{\text{H}\alpha}/M_{\odot}) \approx 10.27$ (Meyer et al., 2004). The $\text{H}\alpha$ -WISE survey (Parkash et al., 2018) further estimates a stellar mass of $\log(M_*/M_{\odot}) \approx 11.2$ and star formation rate of $\log(\text{SFR}/M_{\odot} \text{ yr}^{-1}) \approx 0.58$, placing it near the star-forming main sequence (Whitaker, 2012).

3. Data and Observations

3.1 Radio: EMU

The radio continuum morphology of NGC 5938 as observed with the EMU survey (Hopkins et al., 2025; Norris et al., 2021; Hotan et al., 2021) is presented in Figure 1. The observation was conducted on 21st May 2024 using the full complement of 36 ASKAP antennas, at the central frequency of 943 MHz with a 288 MHz bandwidth (scheduling blocks SB62461). The data were processed using the ASKAPsoft pipelines, including multi-frequency synthesis imaging and multi-scale cleaning. For a complementary view and quantitative analysis of the overall emission, the data were also convolved to a common beam size of $15'' \times 15''$ with a position angle of $\text{PA} = 0$ degrees, from which flux densities were calculated. The higher resolution EMU-HiRES image, as shown in Figure 1, was utilised to effectively illustrate the detailed radio structure of NGC 5938 and to study the centre of the galaxy for the existence of a potential counter jet. Hi-Res processing enhances the visibility of fine details within galaxies, AGN, and other radio sources, as demonstrated by Guzman et al. (2019).

Additionally, we detected NGC 5938 in the Rapid ASKAP Continuum Survey (RACS; McConnell et al., 2020; Hale et al., 2021; Duchesne et al., 2023, 2025) across its Low ($\nu \approx 888 \text{ MHz}$), Mid ($\nu \approx 1367 \text{ MHz}$), and High ($\nu \approx 1655 \text{ MHz}$) frequency bands. RACS provides wide-field continuum imaging with angular resolutions of approximately $15''$ (Low), $12''$ (Mid), and $10''$ (High), and typical sensitivities of $\sim 250\text{--}300 \mu\text{Jy beam}^{-1}$. Measured integrated flux densities for each band are listed in Table 1. In all three RACS bands, NGC 5938 is detected as

a bright, compact radio core coincident with the optical nucleus, accompanied by extended emission associated with the eastern jet region (spans $\sim 33''$). This extended component has integrated flux densities of $4.3 \pm 0.46 \text{ mJy}$ (888 MHz / Low band), $3.0 \pm 0.60 \text{ mJy}$ (1368 MHz / Mid band), and $2.0 \pm 0.69 \text{ mJy}$ (1655 MHz / High band). While the Low band exhibits the highest integrated flux density, consistent with a non-thermal spectrum, the emission morphology is most clearly resolved and detected in the RACS-Mid band (Figure 1). This difference in visual clarity is attributed to the varying angular resolution across the bands. The Low band has the largest beam, which spreads the emission, resulting in lower peak surface brightness and a less distinct morphology, despite having the highest total flux. The detected surface-brightness levels are low, corresponding to only 1.2–1.6 times the RACS rms noise ($\sim 0.25 \text{ mJy beam}^{-1}$). It is important to note that the RACS sensitivity of $\sim 0.25 \text{ mJy beam}^{-1}$ (rms) is roughly five times lower than the EMU survey sensitivity of $\sim 0.05 \text{ mJy beam}^{-1}$. This difference may lead to an underestimation of flux density in RACS, particularly in regions of low surface brightness where faint emission approaches the detection threshold.

Flux densities for the EMU convolved image (SB62461) and the three RACS bands were measured for the jet region, the galaxy centre, and the integrated flux region using Cube Analysis and Rendering Tool for Astronomy (CARTA; Comrie et al., 2021). We used CARTA’s statistical tools to measure the integrated flux density within the elliptical apertures shown in the EMU Convolved Image Figure 1. These apertures were manually defined to enclose the contiguous emission above the local 6σ level for the east jet and the central region, while the galaxy-integrated region encompasses all emission above 3σ . The semi-major axes of these apertures correspond to the characteristic angular extents listed in Table 1.

- Central region: an ellipse with semi-major axis $\sim 32''$ centred on the optical nucleus
- East Jet region: an ellipse with semi-major axis $\sim 33''$, centred on the peak of the eastern extension, encloses the jet-like emission
- Galaxy Integrated region: a larger ellipse with semi-major axis $\sim 176''$ encloses the full galaxy-integrated emission above 3σ level.

Flux density values were extracted using the image statistics panel, and background noise was estimated locally to subtract any baseline offset. No primary beam correction was applied. Flux uncertainties were estimated using the rms noise expressed in mJy beam^{-1} , following the standard relation for uncorrelated noise per synthesised beam:

$$\delta S = \text{rms} \times \sqrt{N_{\text{beam}}}$$

where N_{beam} is the number of synthesised beams within the flux-extraction region,

$$N_{\text{beam}} = A_{\text{flux}}/A_{\text{beam}}$$

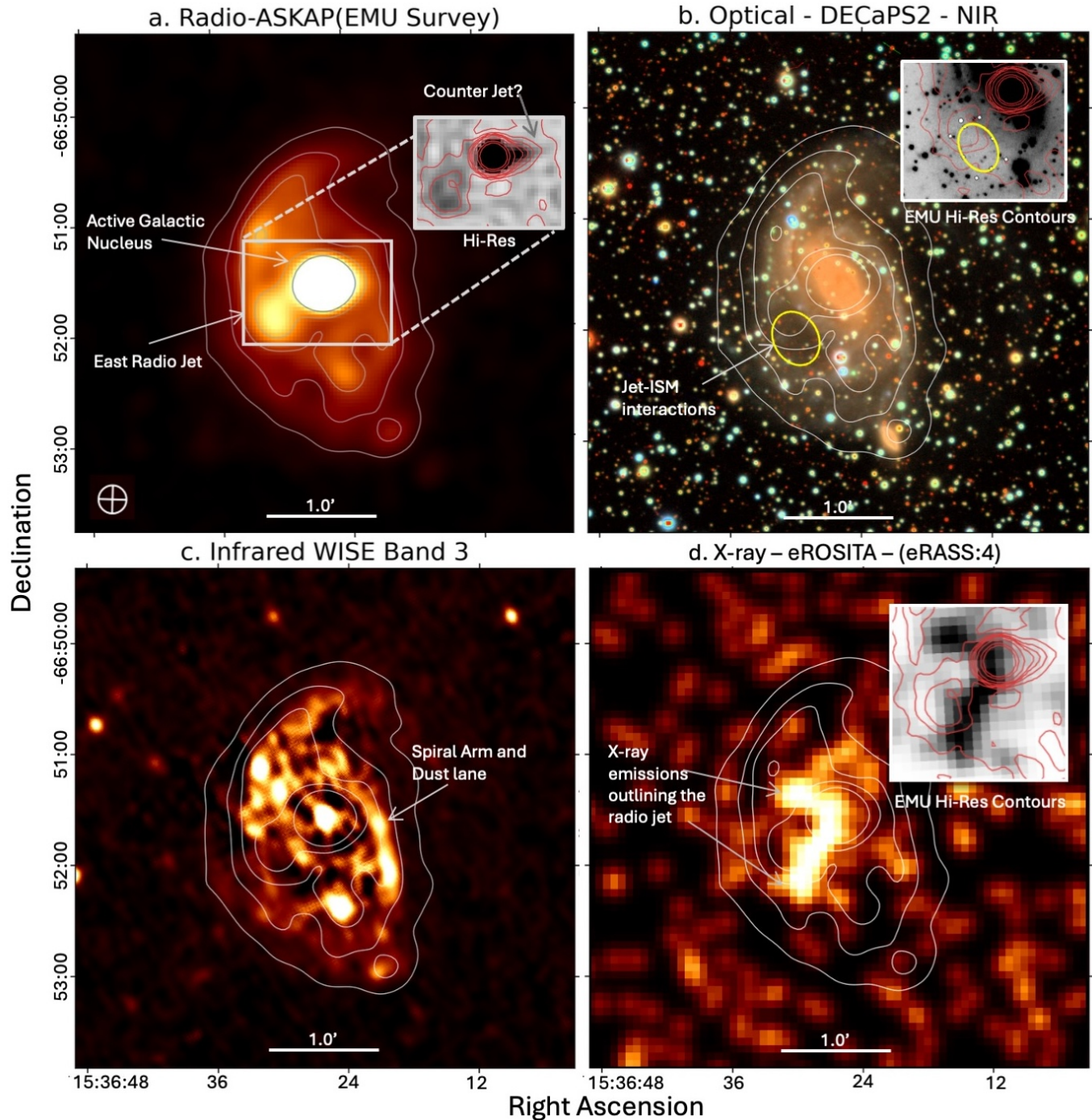


Figure 2. Multi-wavelength observations of the spiral galaxy NGC 5938 (Araish) a: Radio continuum image from EMU 944 MHz tile SB62461, Convolved Image has the beam size of $15''$, at $PA = 0^\circ$, with an EMU Hi-Res inset image showing finer structures of the nucleus. b: DECaPS2 optical/NIR GRZ (475 nm, 644 nm, 926 nm) bands composite image represented by Blue, Green and Red colours respectively, with inset showing Hi-Res radio contours overlaid on the DECaPS2 z-band image, highlighting jet-ISM cavity overlap. c: WISE Band-3. d: eROSITA X-ray Observation: 0.2–5.0 keV, Gaussian smoothing at Full Width at Half Maximum (FWHM)= $3''$, with inset showing Hi-Res radio contours overlaid on X-ray image, highlighting radio jet and X-ray adjoining. The EMU convolved radio contours are applied on all base images at 3, 9, 15, 25, and 50 σ , where $\sigma = 75 \mu\text{Jy beam}^{-1}$. The radio emission from the jet region is encompassed by the 25 σ radio contour.

Table 1. EMU and RACS radio survey flux density and spectral index measurements of regions within NGC 5938.

Frequency ^a (MHz)	East Jet (33'' \approx 4.2 kpc) (mJy)	Centre (32'' \approx 4.1 kpc) (mJy)	Galaxy-Integrated (176'' \approx 22.7 kpc) (mJy)
888 ^L	4.3 \pm 0.46	24.6 \pm 0.44	81.9 \pm 2.44
944 ^E	4.4 \pm 0.09	34.1 \pm 0.09	90.6 \pm 0.49
1368 ^M	3.0 \pm 0.60	21.0 \pm 0.59	49.2 \pm 3.85
1655 ^H	2.0 \pm 0.69	18.9 \pm 0.67	31.8 \pm 3.66
Spectral Index α	-1.2 \pm 0.2	-0.7 \pm 0.4	-1.5 \pm 0.2
888 MHz - Luminosity(W/Hz)	3.7×10^{20}	2.9×10^{21}	7.0×10^{21}
1000 MHz - Luminosity(W/Hz)	3.4×10^{20}	2.2×10^{21}	6.2×10^{21}

^a RMS and beam values for each survey: ^L RACS Low (888 MHz) rms = 0.25 mJy/beam, 15'' beam; ^E EMU (944 MHz) rms = 0.05 mJy/beam, 15'' beam; ^M RACS Mid (1368 MHz) rms = 0.25 mJy/beam, 12'' beam; ^H RACS High (1655 MHz) rms = 0.25 mJy/beam, 10'' beam. Greyed-out values mark RACS flux densities that may be underestimated due to the higher rms noise and lower angular resolution of the RACS data. Flux uncertainties are calculated as $\delta S = \text{rms} \sqrt{N_{\text{beam}}}$.

and A_{beam} is the solid angle area of the synthesized beam.

$$A_{\text{beam}} = \pi \theta_{\text{maj}} \theta_{\text{min}} / (4 \ln 2)$$

This provides the correct noise propagation when integrating flux across extended emission. The measured flux densities and corresponding uncertainties are reported in Table 1, where greyed-out values represent RACS measurements for which the flux density may be underestimated due to the lower angular resolution and higher rms noise of the RACS data, particularly in regions of low surface brightness where emission approaches the detection threshold. We used these flux density measurements to calculate the spectral index (α)^a and the radio luminosity given in (Table 1).

The EMU in-band spectral index of the galaxy's nucleus were also measured using multi-frequency synthesis imaging with Taylor terms T_0 and T_1 . The EMU Taylor images are outputs of the multi-frequency synthesis process, representing the sky brightness as a Taylor series expansion as a function of frequency. The T_0 term corresponds to the intensity image at the reference frequency, while T_1 represents the first-order spectral slope component. The spectral index α for the centre region was derived from the ratio

$$\alpha = \frac{T_1}{T_0},$$

following the approach outlined by [Rau & Cornwell \(2011\)](#). The flux density of the centre region T_0 was measured as 3.72×10^{-2} Jy with a standard deviation of 7.71×10^{-3} Jy beam $^{-1}$, while T_1 was -2.61×10^{-2} Jy with a standard deviation of 5.64×10^{-3} Jy beam $^{-1}$. This results in a spectral index $\alpha = -0.70 \pm 0.21$, indicating a steep spectral slope characteristic of non-thermal emission processes. This result is consistent with the value derived from EMU and RACS flux densities (Table 1). The spectral index is further discussed in Section 4.1. All data are available through the ASKAP Science Data Archive (CASDA)^b.

^aThe spectral index (α) is the logarithmic slope of flux density vs. frequency ($S_{\nu} \propto \nu^{\alpha}$).

^b<https://research.csiro.au/casda>

3.2 Optical/NIR: DECaPS2

Figure 2b shows NGC 5938 in optical and near-IR images from DECaPS2 ([Saydjari et al., 2023](#))^c. The single-exposure limiting magnitudes reach (23.5, 22.6, 21.6) mag in the GRZ (475 nm, 644 nm, 926 nm) bands.

3.3 IR: WISE

Infrared observations (Figures 2c and 3) were obtained from WISE ([Meisner et al., 2022](#)) where band W1, W2, W3, and W4 correspond to 3.4 μ m, 4.6 μ m, 12 μ m, and 22 μ m respectively. Image cutouts were retrieved from Caltech datasets available through the Infrared Science Archive (IRSA) at NASA/I-PAC^d. The WISE AllWISE release provides typical 5 σ point-source sensitivities of 16.5, 15.5, 11.2 and 7.9 mag (Vega) in W1-W4, which correspond to approximate flux density limits of 0.08, 0.11, 1.0 and 6.0 mJy. These sensitivity levels are sufficient to detect faint stellar populations and dust emission in nearby galaxies, although sensitivity degrades in regions of high background noise such as the Galactic plane ([Wright et al., 2010](#)). We also calculated the infrared Vega magnitudes across W1-W4 images as listed in Table 2.

3.4 X-Ray: eROSITA

Figure 2d shows the X-ray image constructed from the combined data from the first four All-Sky Surveys eRASS ([Merloni et al., 2024](#)), eRASS1, eRASS2, eRASS3, and eRASS4, obtained with the eROSITA ([Predehl et al., 2021](#)) onboard the Russian-German SRG mission ([Sunyaev et al., 2021](#)). The eROSITA data were calibrated and cleaned using the pipeline version 020 of the eROSITA Science Analysis Software (eSASS, [Brunner et al. 2022](#), version 20211004). We merged the photon events from all seven telescopes into one event list file for each eRASS. To increase the signal-to-noise ratio, we also generated an event list combining all the data from the four eRASS epochs (hereafter eRASS:4). We applied eRASS:4 (0.2–5.0 keV) image smoothing using a Gaussian kernel with a FWHM of 3'' using the Python Astropy 2D convolution kernel functions.

^cWe use the Legacy Survey Sky browser <https://decaps.legacysurvey.org/>
^d<https://irsa.ipac.caltech.edu/frontpage/>

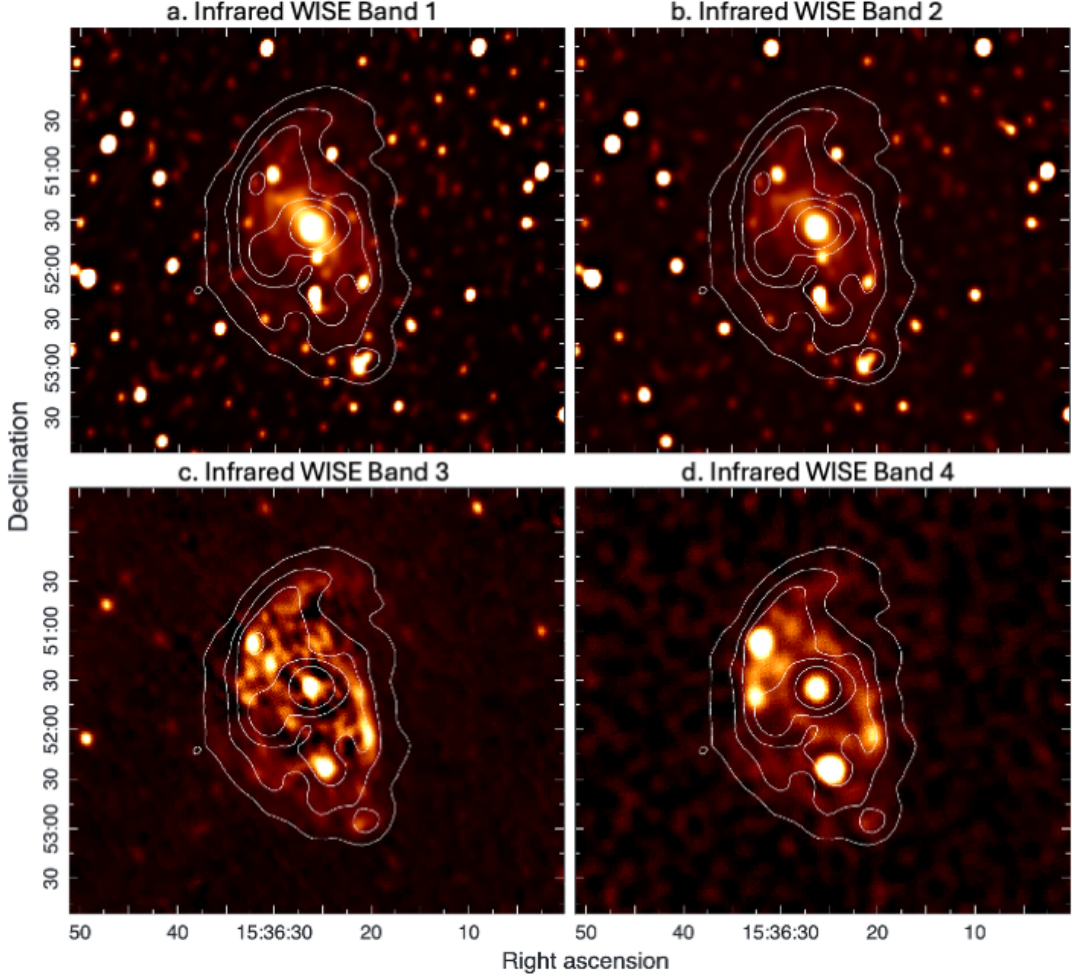


Figure 3. Infrared observations of NGC 5938 a: WISE Band W1, b: Band W2, c: Band W3, d: Band W4 images. 3, 9, 15, 25, and 50 σ contours applied from EMU convolved radio observations, where $\sigma = 75 \mu\text{Jy beam}^{-1}$.

This smoothing scale optimally reveals the features of interest, specifically the X-ray cocoon surrounding the radio emission.

4. Results and Discussion

4.1 Radio Observations

As shown in Figure 1, EMU Hi-Res and Convolved observations, there is an extended region of radio emission perpendicular to the galaxy's major axis, resembling possible AGN jets originating from the central SMBH. Taking the redshift independent distance of ≈ 26.6 Mpc to the galaxy, angular measurements indicate the core to tip length of eastern jet $\approx 40''$ and the total jet extent of the AGN $\approx 64''$, which converts into physical sizes ≈ 5.15 kpc and ≈ 8.2 kpc, respectively. Notably, Figure 2a (Hi-Res Inset image) tentatively labels a feature to the north-west of the nucleus as a “counter jet”. This feature appears to be approximately aligned with the East jet axis but displaced from a direct line of sight, potentially indicating that it is angled out of the plane. Interpretation of this feature include a counter (west) jet, or possibly backflow.

Similar to the well-studied and more energetic galaxy NGC 1068 (Young et al., 2001), which hosts prominent AGN

jets, our observations indicate that the jet is oriented roughly perpendicular to the galactic disk and its major axis. However, this does not definitively establish the jet's 3D orientation relative to the galaxy's actual disk. The jet could be truly perpendicular to the disk, extending directly out of the plane, or it could be inclined at some angle, like in NGC 1068. It is worth noting that in NGC 1068, despite the active AGN, the star formation contributes significantly to the radio emission and the AGN itself accounts for only about half the total radio luminosity (Cecil et al., 2002). If the jet in NGC 5938 is similarly inclined, it may still be propagating through the outer regions of the ISM, rather than through the main disk itself.

Evidence for the jet-ISM interaction, which could help distinguish between these scenarios (Morganti, 2017), is limited in our current data. The optical image (Figure 2b) shows morphological features that are consistent with jet-ISM interaction, though the infrared image (Figure 2c) show no sign of obscuration of the dust lanes, nor any obvious heating of gas or dust along the jet's path. These observations suggest that the jet is likely propagating through relatively low-density ISM, producing subtle structural effects (e.g. a shallow cavity) but without strong radiative or thermal signatures typical of

jet impact on dense molecular gas.

The central AGN region has a spectral index of $\alpha = -0.7 \pm 0.4$, while the eastern jet region shows a steeper index of $\alpha = -1.2 \pm 0.2$. This steeper index suggests a non-thermal emission mechanism, consistent with synchrotron radiation (Filipović & Tothill, 2021). The spectral index of NGC 5938's centre was also calculated using the ratio of EMU Taylor T0 and T1 images; This method gives us the spectral index $\alpha = -0.7 \pm 0.2$, which is consistent with the spectral index calculated using the flux densities from EMU and RACS surveys (Table 1). The observation of radio emission in NGC 5938 extending perpendicular to the galaxy's major axis (Figure 2a), combined with the non-thermal spectral index, strongly supports the interpretation of an AGN jet.

4.2 Optical Observations

The optical observations from DECaPS2 (Figure 2b) show the galaxy in visible light, highlighting the luminous nucleus, distribution of stars and the overall morphology. NGC 5938 is classified as a barred spiral, with a smooth disk and a less prominent central bulge compared to most spiral galaxies, following Moorthy & Holtzman (2006). The dust lanes are apparent in the optical, partially obscuring the galaxy's optical emissions from the nucleus. The DECaPS2 z-band image (Figure 2b) reveals a diffuse stellar and ISM distribution, within which a pronounced under-luminous cavity (highlighted by the yellow ellipse) is identifiable. This cavity appears to be caused by a low density of stars or dust absorption in the region. Although the origin of this cavity is uncertain, it is spatially aligned with the radio-jet axis ($f_{\text{overlap}} \approx 50\%$, white contours). This geometric association suggests a possible imprint of the jet on the surrounding ISM (Morganti, 2017). Such a marginal structural depression would be consistent with a jet propagating through comparatively low-density medium, producing subtle clearing without the strong heating or dust-lane disruption typically associated with jet-ISM interaction in denser regions of galactic disks.

4.3 Infrared Observations

Unlike visible light, infrared emission can pass through dust, making it invaluable for studying obscured star formation and AGN. The longer wavelengths of infrared radiation enable us to detect star formation and AGN that are invisible due to dust blockage in the optical spectrum. It also traces the distribution and properties of the dust itself, a key component of the ISM (Saydjari et al., 2023). NGC 5938 observations from WISE (Wright et al., 2010) W1-W4 bands (Figure 3, Table 2) show prominent infrared emission.

In the W1 band, the galaxy exhibits an apparent magnitude of 8.10 ± 0.02 . For context, Nikutta et al. (2014) shows that WISE sources with $W1 < 11$ are typically dominated by stars, and extragalactic objects become more prevalent at fainter magnitudes, i.e., $W1 > 11^e$. Therefore, our target's W1 magnitude of 8.10 places it firmly among the brightest

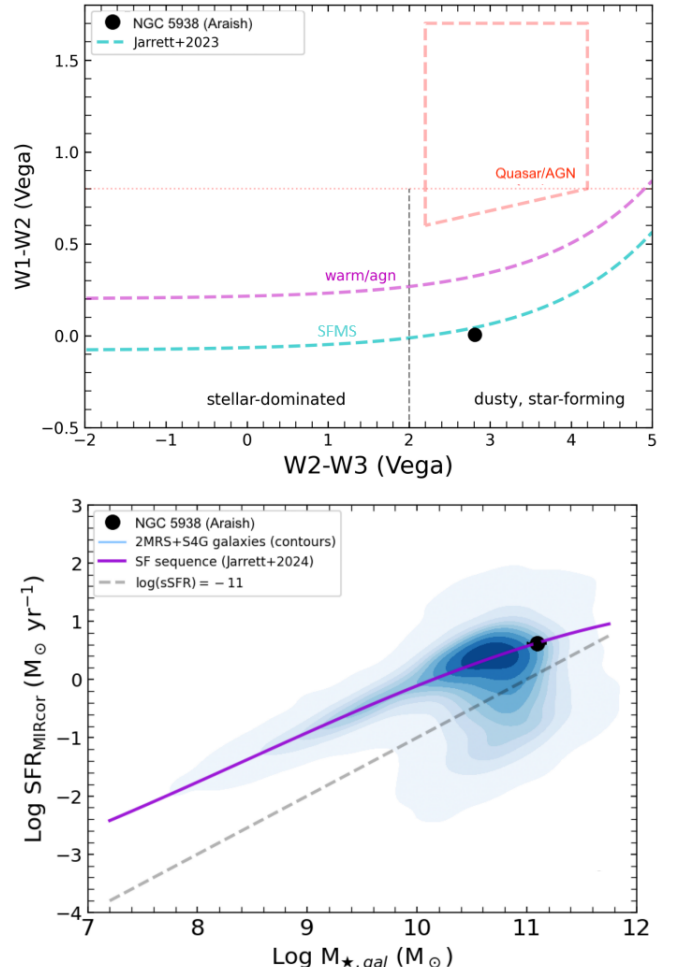


Figure 4. Top: WISE colour-colour diagram showing NGC 5938's position relative to stellar-dominated, dusty star-forming, SFMS, warm/AGN, and Quasar/AGN regions. The dashed curves mark template tracks from Lisenfeld et al. (2023). The location of NGC 5938 (black dot) near the dusty star-forming / warm-AGN boundary indicates the presence of significant dust. Bottom: Star Formation Main Sequence diagram plotting mid-infrared-corrected star formation rate ($\text{SFR}_{\text{MIRcor}}$) derived from WISE 12 μm luminosity following Buzzo et al. (2024) versus stellar mass. The contours represent the distribution of nearby galaxies from the combined 2MRS+S4G sample from Lisenfeld et al. (2023), while the solid magenta line shows the SFMS fit from Buzzo et al. (2024). The dashed grey line corresponds to a specific star formation rate of $\log(\text{sSFR}) = -11 \text{ yr}^{-1}$. NGC 5938 located on the SFMS, consistent with active star formation.

extragalactic objects detected in W1, suggesting a substantial near-infrared luminosity.

Moreover, mid-infrared studies of AGN populations, such as those utilising WISE often focus on sources with W1 magnitudes in the range 10–15 mag i.e. AGN selection criteria by Stern (2012) and O'Connor et al. (2016). Within these samples, an object with $W1 = 8.10$ would be considered exceptionally bright, implying that its infrared emission is significant relative to typical AGN hosts.

Regarding the colours:

- The W1–W2 colour of -0.01 ± 0.04 lies near zero, indicative of a source whose infrared SED is characteristic

^e<https://faculty.washington.edu/ivezic/Publications/WISE1.pdf>

of a cool stellar population with minimal hot dust or AGN torus contribution (Wright et al., 2010).

- The W2–W3 colour of 2.81 ± 0.04 and W3–W4 colour of 2.01 ± 0.05 show significant brightening at longer mid-IR wavelengths, consistent with warm dust emission from star-forming regions and/or lower-luminosity AGN systems (Cluver et al., 2014, 2017).

The position of our target galaxy NGC 5938 (black circle in Figure 4-top panel) on the WISE colour–colour diagram indicates $W1-W2 = -0.01 \pm 0.04$ and $W2-W3 = 2.81 \pm 0.04$. These values place the source below the AGN-dominated region but firmly within the dusty, star-forming locus, consistent with the regime of galaxies exhibiting significant warm dust emission (Lisenfeld et al., 2023). The location also lies above the stellar-dominated sequence, suggesting that mid-infrared emission from heated dust makes a substantial contribution. While its location on the Star Formation Main Sequence (SFMS) in Figure 4-bottom panel confirms its classification as a star forming galaxy (Brinchmann et al., 2004), where its star formation rate $\log SFR [M_{\odot} \text{ yr}^{-1}] = 0.58 \pm 0.08$ is obtained from (Buzzo et al., 2024) and the stellar mass $\log M* = 11.24 \pm 0.10$ is taken from Parkash et al. (2018).

The presence of cool dust around the centre of the NGC 5938, as indicated by W2–W3 colour, could be due to interactions between high-velocity particles in AGN jets and the interstellar dust grains (Cielo et al., 2017; Cluver et al., 2014). However, it is important to note that in the W1–W3–W4 RGB image (Figure 5), we do not observe any increase in infrared emission, disturbance in dust distribution, or other signs of jet–ISM interaction coincident with the radio jet’s location. No other prominent infrared sources are detected within $6''$ of the radio jet. The native angular resolution of WISE is $\sim 6''$ in W1–W3 and $\sim 12''$ in W4 (Wright et al., 2010), which is sufficient to trace global dust emission but not to resolve small-scale interactions between the radio jet and the interstellar dust. Thus, the observed WISE colours provide evidence for cool dust in the galaxy, although higher-resolution infrared data would be required to directly probe any jet–ISM interaction.

Table 2. Infrared Magnitude - WISE

WISE Bands	Magnitude (Vega)	Magnitude (AB)
W1	8.10 ± 0.02	10.80 ± 0.02
W2	8.11 ± 0.04	11.45 ± 0.04
W3	5.30 ± 0.06	10.54 ± 0.06
W4	3.29 ± 0.08	9.89 ± 0.08
W1–W2	-0.01 ± 0.04	-0.65 ± 0.04
W2–W3	2.81 ± 0.04	0.91 ± 0.04
W3–W4	2.01 ± 0.05	0.65 ± 0.05
Surface Brightness	17.437	
$\log M^* [M_{\odot}]$	11.24 ± 0.10	
$\log SFR [M_{\odot} \text{ Year}^{-1}]$	0.58 ± 0.08	

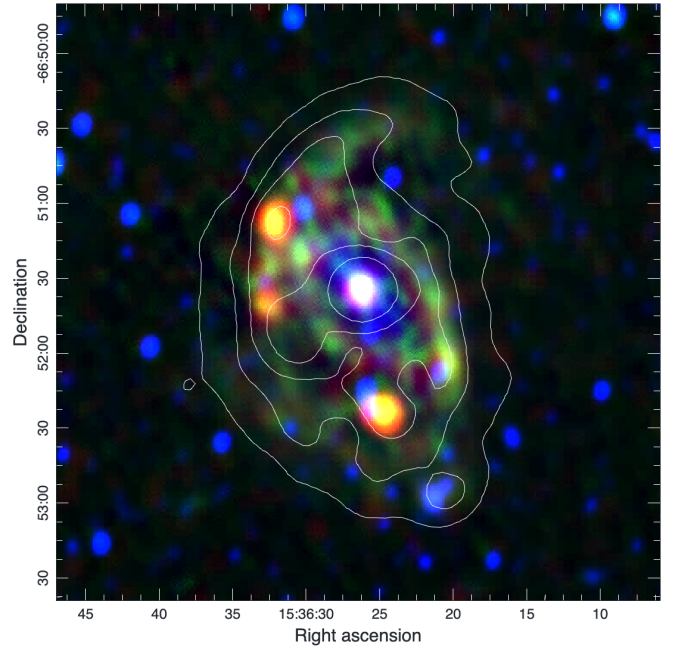


Figure 5. RGB WISE Red-W4, Green-W3, and Blue-W1. W1 colour indicates excess hot dust emission from an AGN while W3 and W4 luminosity is sensitive to star formation. Radio Contours 3, 9, 15, 25, and 50 σ applied from EMU radio observations.

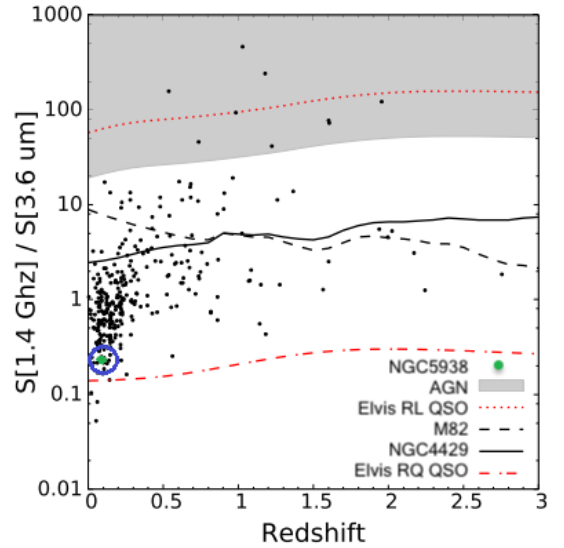


Figure 6. The ratio between the radio 1.4 GHz and extrapolated $3.6 \mu\text{m}$ integrated flux density plotted as a function of redshift. Black points represent galaxies from Weston et al. (2018). The green circled dot marks the flux density ratio of NGC 5938 (this work). The grey shaded area denotes the loci of radio-loud AGN as per Weston et al. (2018). Template tracks are shown for the starburst galaxy M82 (black dashed line), and the spiral galaxy NGC 4429 (black solid line) from Seymour et al. (2007), radio-loud quasars (red dotted line), and radio-quiet quasars (red dash-dotted line) from Elvis et al. (1994).

4.3.1 Infrared and Radio Emission Analysis

To further investigate AGN activity in NGC 5938, we calculated the radio-to-infrared flux density ratio, a valuable diagnostic tool commonly used in identifying AGN jets (Weston et al., 2018). This ratio was computed using the integrated radio flux density at 1.4 GHz (Table 1) and infrared flux density at 3.6 μm to generate the ratio. We used the integrated radio flux density at 944 MHz, $S_{944} = 90.6 \pm 0.49 \text{ mJy}$ (Table 1), and the measured spectral index $\alpha = -1.5 \pm 0.2$ to extrapolate flux density at 1.4 GHz using the power-law relation (Equation 1), yielding $S_{1.4} = 50.16 \pm 4.27 \text{ mJy}$.

$$S_2 = S_1 \left(\frac{v_2}{v_1} \right)^\alpha \quad (1)$$

For infrared measurements, the WISE W1 Vega magnitude of $M_{W1} = 8.10 \pm 0.02$ was converted to a flux density (Equation 2; Wright et al., 2010), where $S_{v_0} = 306.7 \text{ Jy}$ is the W1 zero-magnitude flux density (Wright et al., 2010). This yields $S_{3.6} = 176.48 \pm 4.0 \text{ mJy}$. Extrapolating to 3.6 μm using the measured infrared spectral index ($\alpha_{\text{IR}} \approx -1.0$) gives $S_{3.6} \approx 209.5 \pm 4.0 \text{ mJy}$.

$$S_{W1} = S_{v_0} \times 10^{-0.4 \times M_{W1}} \quad (2)$$

$$R_{1.4/3.6} = \frac{S_{1.4, \text{GHz}}}{S_{3.6, \mu\text{m}}} \quad (3)$$

The radio-to-infrared ratio (Equation 3) is 0.24 ± 0.02 , which lies well below the canonical radio-loud quasar threshold ($R > 10$; Elvis et al. 1994), indicating that radio emission is not the dominant power source. In Figure 6, NGC 5938 (green dot) lies marginally above the median star-forming galaxy locus but well below the radio-loud AGN regime.

To place this ratio in a broader context, we compared NGC 5938's stellar mass ($\log M_*/M_\odot = 11.02 \pm 0.05$) and radio luminosity at 888 MHz ($\log L_{888\text{MHz}} = 21.50 \pm 0.03 \text{ W Hz}^{-1}$) to the distributions of AGN hosts identified using optical Baldwin, Phillips & Terlevich (BPT) diagnostics, WISE colours, the Mass-Excitation diagram, and ProSpect(0010) modelling from Prathap et al. (2024). While the radio-to-infrared ratio alone would not classify NGC 5938 as strongly radio-loud, its radio luminosity is consistent with the median values for AGN selected by ProSpect(0010), a method designed to detect lower-luminosity AGN in massive hosts.

This quantitative cross-comparison indicates that NGC 5938 likely harbours a low luminosity AGN where radio output is modest compared to its infrared emission, though consistent with multi-wavelength AGN diagnostics. The results emphasise that in composite systems, where star formation and AGN activity both contribute to the observed flux, a single diagnostic can under-represent the AGN component, and multi-method analyses are required for reliable classification.

4.4 X-ray Observations

4.4.1 X-ray emission from the radio jet

In the X-ray regime, we investigated the galaxy NGC 5938 utilising the eROSITA-eRASS:4 X-ray 0.2–5.0 keV processed

image (Figure 2d). Using the `ermldet` task, no strong point-like X-ray source was detected at the radio jet's position. Instead, the observed X-ray morphology reveals extended, diffuse emission broadly following the radio contours (Figure 2d, Figure 7), consistent with a cocoon of shocked gas surrounding the jet. To quantify this, we extracted photons within the 3σ radio contour, detecting 29 counts (4 background) in the 0.2–2.3 keV band, corresponding to a significance $> 3\sigma$.

To estimate the X-ray upper limit of the jet region, we extracted X-ray spectra using `srctool` with a $10''$ circular region centred at the position of the east radio jet (EEF = 0.4; Tubín-Arenas et al. 2024) and an annulus ($70''$ – $130''$) for background subtraction. Following Kraft et al. (1991), assuming a power-law spectrum with galactic absorption ($N_{\text{H}} = 1.4 \times 10^{21} \text{ cm}^{-2}$) and photon index $\Gamma = 1.8$, we obtained a 3σ flux upper limit of $S_{0.2-2.0\text{keV}} \approx 0.7 \times 10^{-13} \text{ erg cm}^{-2} \text{ s}^{-1}$, resulting in a soft X-ray luminosity of $L_{\text{X}} \approx 6.0 \times 10^{39} \text{ erg s}^{-1}$ ($\log L_{\text{X}} \approx 39.8$).

To assess the possibility of a central AGN, we extracted the X-ray events from a $10''$ circular region centred at the core (Figure 7). This yielded 7 photons (0.7 background), significant at $> 3\sigma$. However, all photons fall below (2 keV), with no hard X-rays ($\geq 2 \text{ keV}$) detected. As a result, the inferred luminosity pertains only to the soft X-ray band. Due to the low photon counts, we estimated the soft X-ray flux assuming an absorbed power-law model ($N_{\text{H}} = 1.4 \times 10^{21} \text{ cm}^{-2}$ and $\Gamma = 1.8$). The resulting soft X-ray luminosity ($3.4 \pm 3 \times 10^{39} \text{ erg s}^{-1}$) is consistent with LINER galaxies ($\log L_{\text{X}} \approx 39.9$) and higher than HII galaxies ($\log L_{\text{X}} \approx 39.3$), while remaining well below the typical Seyfert regime ($\log L_{\text{X}} \approx 41.0$, Georgantopoulos et al., 1999). Notably, this luminosity is also broadly consistent with empirical relations for X-ray binary (XRB) populations and shock-heated plasma in a galaxy with an $\text{SFR} \approx 0.58 M_\odot/\text{yr}$ (Mineo et al., 2012; Ranalli et al., 2003). This suggests that the observed soft emission may be dominated by stellar processes and shock-heated gas associated with the radio-jet interaction rather than the AGN itself.

Although no hard-band emission is detected, we evaluated whether NGC 5938 could host a heavily obscured near-Compton-thick AGN (Ricci et al., 2015). We derived 3σ upper limits from the eROSITA data, assuming a heavily obscured power-law model with $N_{\text{H}} \gtrsim 1.0 \times 10^{24} \text{ cm}^{-2}$ and $\Gamma = 1.8$. This observed hard-band upper limit corresponds to an intrinsic luminosity limit of $L_{2-10\text{keV}} \lesssim 6.8 \times 10^{42} \text{ erg s}^{-1}$, with a corresponding soft-band intrinsic limit of $L_{0.2-2\text{keV}} \lesssim 6.6 \times 10^{42} \text{ erg s}^{-1}$. These limits, along with the estimated soft X-ray luminosity under low absorption scenario, imply that NGC 5938 does not host a luminous Seyfert-like AGN, and that any nuclear activity is either intrinsically weak or heavily absorbed (Gilli et al., 2007; Brightman & Nandra, 2012; Ricci et al., 2015). Comparison with the BASS survey (Tokayer et al., 2025) further shows that NGC 5938 is significantly less luminous and lacks the detectable hard X-ray emissions ($\log L_{14-195\text{keV}} \geq 43$), characteristics of the powerful AGN

probed in the study [Tokayer et al. \(2025\)](#).

Although more complex absorption scenarios, such as highly ionised absorbers, could in principle suppress the hard band while allowing some soft emission ([Done et al., 2007](#)); however the limited signal-to-noise ratio of the available data prevents any meaningful constraints on these models. These results are consistent with a scenario in which the AGN in NGC 5938 may be undergoing a low-accretion-rate, *pre-blowout* phase, where the nuclear feedback is currently insufficient to clear the surrounding obscuring material. We therefore conclude that the current data cannot rule out a deeply buried, low-luminosity nucleus, although the observed emission is more naturally explained by non-AGN processes. Deeper hard X-ray observations (e.g. with *NuSTAR*; [Harrison et al. 2013](#)) would be required to detect or place meaningful constraint on any obscured nuclear emission.

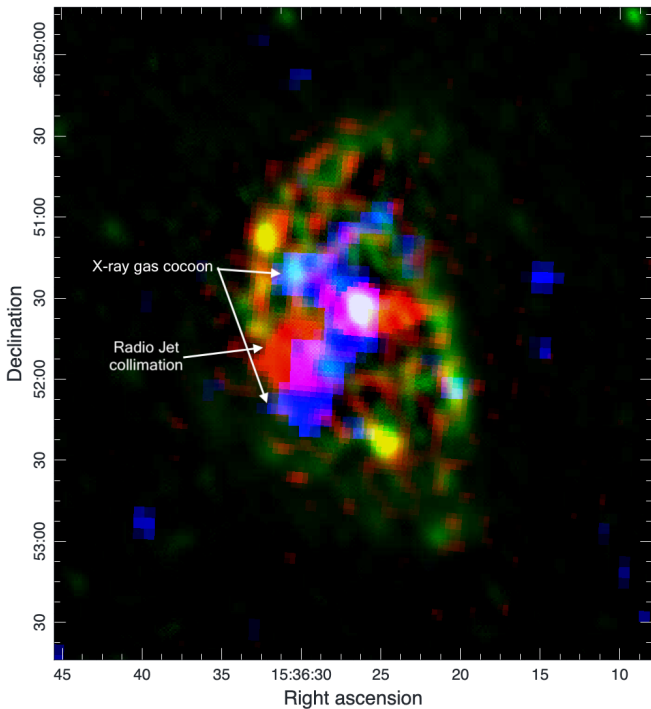


Figure 7. RGB composite image of NGC 5938 illustrating the distribution of radio emission (Red)-EMU Hi-Res, infrared W3 emission (Green)-WISE and X-ray emission (Blue) - eROSITA. The radio jet seems to be collimated by the surrounding X-ray gas.

4.4.2 X-Ray and Radio Emission Interplay

Focusing on the centre of the galaxy's nucleus, the X-ray continuum image (Figure 2d) reveals **emission concentrated towards** the galaxy's nucleus, as further delineated by the overlaid radio contours. The observed X-ray jet-like emission could originate from the superheated gas spiralling towards a supermassive black hole or outflows often associated with AGN activity ([Filipović & Tothill, 2021](#)). However, the relationship between the extended X-ray gas and radio halo is complex. While at a glance, the multi-frequency composite

(Figure 7 radio emission is shown in red, X-ray emission in blue) image might visually suggest a less direct spatial overlap, a closer examination (Figure 2d inset) reveals that the brighter X-ray emission is primarily adjacent to and often outlines the radio contours, especially towards the south-east. This diffuse and enveloping morphology indicates that the radio jet is likely interacting with, and potentially confined by, the more extended X-ray gas/halo.

Similar to the systems like ESO 295-IG022 ([Read et al., 2001](#)), Centaurus A ([Feigelson, 1982](#)), UGCA 127 (Phaedra, [Filipović et al., 2025](#)) and NGC 1068 ([Young et al., 2001](#)), where jet-ISM interactions are prominent, the X-ray emission in NGC 5938 might be indicative of diffuse, shocked gas at the jet's edge and along its boundaries. While Centaurus A exhibits X-ray cavities, it also shows significant X-ray emissions from shocks at the edge of its lobes. Similarly NGC 1068 displays X-ray features linked to direct jet-cloud impacts and shocks. Therefore, in the case of NGC 5938, in addition to potentially larger-scale confinement or channelling, the observed X-ray morphology suggests the possibility of shocked emission due to the jet's interaction with the surrounding medium at the boundary. This interaction could be similar to the "cocoon" effect seen in ESO 295-IG022, where the jets may be collimated by the surrounding X-ray gas, maintaining pressure balance between the central ISM and the gas within the jet. This would also be very suggestive of channelling effects taking place, whereby the violent radio continuum jets can punch holes and displace the X-ray emitting cluster gas, as is also seen in the NGC 1275 jet at the centre of the Perseus cluster ([Gendron-Marsolais et al., 2021](#)).

5. Conclusion

Here we presented a multi-frequency study of the barred spiral galaxy NGC 5938 (Araish), leveraging new EMU and RACS surveys data. Our analysis reveals the presence of extended, steep spectrum radio emission with a spectral index of $\alpha = -1.2 \pm 0.2$ suggesting synchrotron emission indicative of an AGN jet. The radio jet extends perpendicular to the galaxy's major axis, reaching a physical size of ≈ 8.2 kpc. The galaxy's nucleus has a spectral index ($\alpha = -0.7 \pm 0.4$), consistent with the signature of core AGN activity ([Stern, 2012](#)).

The host galaxy is found to lie on the star-forming main sequence, and WISE colour diagnostics place it firmly within the star-forming regime, with no indication of a classical quasar-like AGN. However, the radio-to-infrared flux ratio places NGC 5938 in a region occupied by radio-quiet quasars, this finding is critically consistent with the recognised continuum of radio activity, in which many systems exhibit composite radio output from low luminosity jets and/or compact cores together with star-formation-related emission i.e. "radio-intermediate" or low-excitation/low-luminosity AGN ([Best & Heckman, 2012](#)).

The X-ray properties of NGC 5938 provide further insight into this composite nature. X-ray emission from the galaxy's nucleus aligns with the radio contours, suggesting a concentrated source. The soft X-ray luminosity

($L_X \approx 3.4 \times 10^{39} \text{ ergs}^{-1}$) is consistent with that expected from X-ray binary populations and shock-heated plasma for the galaxy's star-formation rate (SFR $\approx 0.58 M_\odot/\text{yr}$). While the absence of hard X-ray emission ($\geq 2 \text{ keV}$) disfavours a luminous, unobscured AGN, our analysis of the 2–10 keV upper limits suggests that a deeply buried or low-accretion-rate nucleus cannot be ruled out. Such a system may be in a ‘pre-blowout’ phase, where nuclear feedback is insufficient to clear the surrounding obscuring material. Crucially, the observed spatial relationship, where the X-ray outlining follows the extended radio jet (similar to systems like ESO 295-IG022, Centaurus A, and NGC 1068), is highly suggestive of jet confinement and channelling effects caused by the surrounding X-ray gas or halo. This displacement of the X-ray emitting gas by the radio jets, a phenomenon seen in systems such as NGC 1275, supports a scenario where the jet is being collimated.

The barred spiral morphology of NGC 5938 likely contributes to the funnelling of gas towards the central black hole (Galloway et al., 2015), enhancing accretion and powering the observed AGN activity. While the optical morphology suggests possible interaction of the jet with the host galaxy's interstellar medium, current infrared data provide no direct evidence of strong jet-ISM coupling.

It is critical to acknowledge that identifying AGN and disentangling their contributions from star formation remains a significant challenge. Different selection methods can reveal AGN populations with varying characteristics, introducing potential selection biases. This interplay remains tentative and will require multi-band follow-up to confirm. To fully constrain the physical parameters driving jet confinement, future work should prioritize higher-resolution radio observations and deeper hard X-ray spectral modelling (e.g., with NuSTAR) to accurately map the thermal and pressure structure of the surrounding medium.

The combination of an active central engine producing a synchrotron jet and a disk galaxy with ongoing star formation firmly establishes NGC 5938 as a compelling new example of a spiral DRAGN. It represents a crucial laboratory for studying the effects of AGN-driven jets in non-elliptical hosts, offering unique insights into feedback mechanisms in disk-dominated galaxies. This case study highlights the power of the EMU survey in uncovering rare, unusual galaxies when combined with multi-wavelength ancillary data, and underscores the potential for future systematic searches to identify further spiral DRAGNs and constrain their role in galaxy evolution.

Acknowledgement

This scientific work uses data obtained from Inyarrimanha Ilgari Bundara/the Murchison Radio-astronomy Observatory. We acknowledge the Wajarri Yamaji People as the Traditional Owners and native title holders of the Observatory site. CSIRO's ASKAP radio telescope is part of the Australia Telescope National Facility (<https://ror.org/05qajvd42>). Operation of ASKAP is funded by the Australian Government with support from the National Collaborative Research Infra-

structure Strategy. ASKAP uses the resources of the Pawsey Supercomputing Research Centre. Establishment of ASKAP, Inyarrimanha Ilgari Bundara, the CSIRO Murchison Radio-astronomy Observatory and the Pawsey Supercomputing Research Centre are initiatives of the Australian Government, with support from the Government of Western Australia and the Science and Industry Endowment Fund.

This work is also based on data from eROSITA, the soft X-ray instrument aboard SRG, a joint Russian-German science mission supported by the Russian Space Agency (Roscosmos), in the interests of the Russian Academy of Sciences represented by its Space Research Institute (IKI), and the Deutsches Zentrum für Luft- und Raumfahrt (DLR). The SRG spacecraft was built by Lavochkin Association (NPOL) and its subcontractors, and is operated by NPOL with support from the Max-Planck Institute for Extraterrestrial Physics (MPE). The development and construction of the eROSITA X-ray instrument was led by MPE, with contributions from the Dr. Karl Remeis Observatory Bamberg, the University of Hamburg Observatory, the Leibniz Institute for Astrophysics Potsdam (AIP), and the Institute for Astronomy and Astrophysics of the University of Tübingen, with the support of DLR and the Max Planck Society. The Argelander Institute for Astronomy of the University of Bonn and the Ludwig Maximilians Universität Munich also participated in the science preparation for eROSITA. The eROSITA data shown here were processed using the eSASS/NRTA software system developed by the German eROSITA consortium.

M.D.F. and S.L. acknowledge Australian Research Council (ARC) funding through grant DP200100784.

T.A. acknowledges the support from the National SKA Program of China (2022SKA0120102), FAST special funding (NSFC 12041301), and the Xinjiang Tianchi Talent Program.

References

- Best, P. N., & Heckman, T. M. 2012, MNRAS, 421, 1569
- Brightman, M., & Nandra, K. 2012, Monthly Notices of the Royal Astronomical Society, 422, 1166
- Brinchmann, J., Charlot, S., White, S. D. M., et al. 2004, Monthly Notices of the Royal Astronomical Society, 351, 1151
- Brunner, H., Liu, T., Lamer, G., et al. 2022, A&A, 661, A1
- Buzzo, M. L., Forbes, D. A., Jarrett, T. H., et al. 2024, MNRAS, 529, 3210
- Cecil, G., Bland-Hawthorn, J., Veilleux, S., & Filippenko, A. V. 2001, The Astrophysical Journal, 555, 338
- . 2002, The Astronomical Journal, 120, 367
- Cielo, S., Antonuccio-Delogu, V., Silk, J., & Romeo, A. D. 2017, Monthly Notices of the Royal Astronomical Society, 467, 4526
- Cluver, M. E., Jarrett, T. H., Dale, D. A., & et al. 2014, ApJ, 782, 90
- Cluver, M. E., Jarrett, T. H., Dale, D. A., et al. 2017, The Astrophysical Journal, 850, 68
- Comrie, A., Wang, K.-S., Hsu, S.-C., et al. 2021, CARTA: Cube Analysis and Rendering Tool for Astronomy, Astrophysics Source Code Library, record ascl:2103.031, doi:10.5281/zenodo.4034416
- Done, C., Gierliński, M., & Kubota, A. 2007, The Astronomy and Astrophysics Review, 15, 1–66
- Doyle, M. T., Drinkwater, M. J., Rohde, D. J., et al. 2005, MNRAS, 361, 34
- Duchesne, S. W., Thomson, A. J. M., Pritchard, J., et al. 2023, PASA, 40, e034
- Duchesne, S. W., Ross, K., Thomson, A. J. M., et al. 2025, PASA, 42, e038
- Elmouttie, M., Haynes, R. F., Jones, K. L., Sadler, E. M., & Ehle, M. 1998, MNRAS, 297, 1202

Elvis, M., Wilkes, B. J., McDowell, J. C., et al. 1994, *ApJS*, 95, 1

Fabian, A. C. 2012, *ARA&A*, 50, 455

Feigelson, E. D. 1982, in IAU Symposium, Vol. 97, Extragalactic Radio Sources, ed. D. S. Heeschen & C. M. Wade, 107–114

Filipović, M. D., Smeaton, Z. J., Bradley, A. C., et al. 2025, *ApJ*, 984, L52

Filipović, M. D., & Tothill, N. F. H., eds. 2021, *Multimessenger Astronomy in Practice* (IOP Publishing), doi:10.1088/2514-3433/ac2256

Galloway, M. A., Willett, K. W., Fortson, L. F., et al. 2015, *Monthly Notices of the Royal Astronomical Society*, 448, 3442

Gao, X. Y., Yuan, Z. S., Han, J. L., Wen, Z. L., & Shan, S. S. 2023, *Research in Astronomy and Astrophysics*, 23, 035005

Gendron-Marsolais, M. L., Hull, C. L. H., Perley, R., et al. 2021, *ApJ*, 911, 56

Georgantopoulos, I., Basilakos, S., & Plionis, M. 1999, *Monthly Notices of the Royal Astronomical Society*, 305, 125

Gilli, R., Comastri, A., & Hasinger, G. 2007, *Astronomy & Astrophysics*, 463, 79

Guzman, J., Whiting, M., Voronkov, M., et al. 2019, ASKAPsoft: ASKAP science data processor software, *Astrophysics Source Code Library*, doi:10.5281/zenodo.3563914

Hale, C. L., McConnell, D., Thomson, A. J. M., et al. 2021, *Publications of the Astronomical Society of Australia*, 38, doi:10.1017/pasa.2021.47

Harrison, F. A., Craig, W. W., Christensen, F. E., et al. 2013, *The Astrophysical Journal*, 770, 103

Hopkins, A. M., Kapinska, A., Marvil, J., et al. 2025, *The Evolutionary Map of the Universe: A new radio atlas for the southern hemisphere sky*, arXiv:2505.08271

Hotan, A. W., Bunton, J. D., Chippendale, A. P., et al. 2021, *PASA*, 38, doi:10.1017/pasa.2021.1

Koribalski, B. S., Staveley-Smith, L., Kilborn, V. A., et al. 2004, *AJ*, 128, 16

Kraft, R. P., Burrows, D. N., & Nousek, J. A. 1991, *ApJ*, 374, 344

Ledlow, M. J., Owen, F. N., Yun, M. S., & Hill, J. M. 2001, *The Astrophysical Journal*, 552, 120

Lisenfeld, U., Ogle, P. M., Appleton, P. N., Jarrett, T. H., & Moncada-Cuadri, B. M. 2023, *A&A*, 673, A87

Mao, M. Y., Blanchard, J. M., Owen, F., et al. 2018, *Monthly Notices of the Royal Astronomical Society: Letters*, 478, L99

Mauch, T., & Sadler, E. M. 2007, *MNRAS*, 375, 931

McConnell, D., Hale, C. L., Lenc, E., et al. 2020, *PASA*, 37, e048

Meisner, A. M., Lang, D., Schlafly, E. F., & Schlegel, D. J. 2022, *Research Notes of the American Astronomical Society*, 6, 188

Merloni, A., Lamer, G., Liu, T., et al. 2024, *A&A*, 682, A34

Meyer, M. J., Zwaan, M. A., Webster, R. L., et al. 2004, *MNRAS*, 350, 1195

Mineo, S., Gilfanov, M., & Sunyaev, R. 2012, *Monthly Notices of the Royal Astronomical Society*, 419, 2095

Moorthy, B. K., & Holtzman, J. A. 2006, *MNRAS*, 371, 583

Morganti, R. 2017, *Frontiers in Astronomy and Space Sciences*, 4, doi:10.3389/fspas.2017.00042

Nikutta, R., Hunt-Walker, N., Nenkova, M., Ivezić, v., & Elitzur, M. 2014, *Monthly Notices of the Royal Astronomical Society*, 442, 3361

Norris, R. P., Marvil, J., Collier, J. D., et al. 2021, *PASA*, 38, e046

Norris, R. P., Yew, M., Crawford, E., et al. 2025, *EMU and the DRAGNs I: A Catalogue of DRAGNs*, arXiv:2507.23337

O'Connor, J. A., Rosenberg, J. L., Satyapal, S., & Secret, N. J. 2016, *Monthly Notices of the Royal Astronomical Society*, 000, 1

Parkash, V., Brown, M. J. I., Jarrett, T. H., & Bonne, N. J. 2018, *The Astrophysical Journal*, 864, 40

Parkash, V., Brown, M. J. I., Jarrett, T. H., & Bonne, N. J. 2018, *ApJ*, 864, 40

Prathap, J., Hopkins, A. M., Robotham, A. S. G., et al. 2024, *PASA*, 41, e016

Predehl, P., Andritschke, R., Arefiev, V., et al. 2021, *A&A*, 647, A1

Ranalli, P., Comastri, A., & Setti, G. 2003, *Astronomy & Astrophysics*, 399, 39

Rau, U., & Cornwell, T. J. 2011, *Astronomy & Astrophysics*, 532, A71

Read, A. M., Filipović, M. D., Pietsch, W., & Jones, P. A. 2001, *A&A*, 369, 467

Ricci, C., Ueda, Y., Koss, M. J., et al. 2015, *ApJ*, 815, L13

Saydari, A. K., Schlafly, E. F., Lang, D., et al. 2023, *The Astrophysical Journal Supplement Series*, 264, 28

Seymour, N., Stern, D., De Breuck, C., et al. 2007, *The Astrophysical Journal Supplement Series*, 171, 353

Singh, V., Ishwara-Chandra, C. H., Sievers, J., et al. 2015, *Monthly Notices of the Royal Astronomical Society*, 454, 1556

Steer, I. 2020, *AJ*, 160, 199

Stern, D. 2012, *ApJ*, 753, 30

Sunyaev, R., Arefiev, V., Babyshkin, V., et al. 2021, *A&A*, 656, A132

Terry, J. N., Paturel, G., & Ekholm, T. 2002, *A&A*, 393, 57

Theureau, G., Hanski, M. O., Coudreau, N., Hallet, N., & Martin, J. M. 2007, *A&A*, 465, 71

Tokayer, Y. M., Koss, M. J., Urry, C. M., et al. 2025, *The Astrophysical Journal*, 982, arXiv:2501.16708

Tubín-Arenas, D., Krumpe, M., Lamer, G., et al. 2024, *A&A*, 682, A35

Weston, S. D., Seymour, N., Gulyaev, S., et al. 2018, *MNRAS*, 473, 4523

Whitaker, K. E. e. a. 2012, *ApJ*, 754, L29

Wright, E. L., Eisenhardt, P. R. M., Mainzer, A. K., et al. 2010, *AJ*, 140, 1868

Young, A. J., Wilson, A. S., & Shopbell, P. L. 2001, *The Astrophysical Journal*, 556, 6